Journal of Power Sources 211 (2012) 46–51

Contents lists available at SciVerse ScienceDirect

Journal of Power Sources

journal homepage: www.elsevier.com/locate/jpowsour

Stable high areal capacity lithium-ion battery anodes based on three-dimensional Ni–Sn nanowire networks

Miao Tian [a], Wei Wang [a], Yujie Wei [b], Ronggui Yang [a,*]

[a] Department of Mechanical Engineering, University of Colorado, ECME 273, 427 UCB, Boulder, CO 80309, USA
[b] State Key Laboratory of Nonlinear Mechanics, Institute of Mechanics, Chinese Academy of Sciences, Beijing 100190, PR China

ARTICLE INFO

Article history:
Received 14 February 2012
Received in revised form
22 March 2012
Accepted 23 March 2012
Available online 11 April 2012

Keywords:
Lithium-ion battery
Nanowire electrode
Ni–Sn alloy
Nanowire network
Areal capacity

ABSTRACT

Nanowire arrays present an excellent candidate for high performance lithium-ion battery electrodes. However, agglomeration in long nanowire arrays impedes nanowire-based electrodes from delivering high areal capacity, by degrading the nanoscale wires to micro-sized bundles and reducing the mechanical stability. In this study, we develop a simple way to fabricate three-dimensional (3D) nickel–tin (Ni–Sn) nanowire networks by using 3D porous anodic alumina templates synthesized from low-cost impure aluminum foils. By eliminating agglomeration, stable high areal capacity anodes are demonstrated with 3D self-supporting Ni–Sn nanowire network structures. With a nanowire length of 40 μm, the 3D Ni–Sn nanowire networks can deliver an areal capacity as high as 4.3 mAh cm^{-2} with a cycle life longer than 50 cycles. The 3D Ni–Sn nanowire networks also exhibit an excellent rate capability with 72% of the capacity retained when the test rate increases from C/5 to 6C.

1. Introduction

Lithium-ion (Li-ion) batteries have become the leading energy source for various applications from smartphones and laptops to electric vehicles [1–4]. Recently, there has been tremendous interest and effort in using nanowire arrays as electrodes for high capacity and high power Li-ion batteries. There are many advantages to using nanowire arrays as battery electrodes [5–8]: (1) the spaces between nanowires provide not only easy access of electrolyte to active materials but also efficient volume-change accommodation during the charging/discharging processes; (2) the large specific surface area and the small diameter of nanowires facilitate Li-ion reaction with electrodes; (3) the direct connection of nanowires to the current collector allows efficient electron flow after electrons being generated, which eliminates the necessity of binder materials or conducting additives [9–13]. For example, gravimetric capacity higher than 1000 mAh g^{-1} with ~90% capacity retention over 100 cycles has been recently realized by using Si nanowires [14]. Despite the promising improvements, low mass loading of active materials and low areal capacity still limits straight nanowire arrays as battery electrodes [15–19]. The areal capacity of straight nanowire array electrodes could potentially be increased by increasing the length of the nanowires [20]. However, the high aspect ratio of long nanowires leads to agglomeration, which can significantly degrade the electrochemical performance of nanowire array electrodes due to the reduced surface area, blocked Li-ion diffusion, and the increased stress in the agglomerated nanowire arrays.

Nickel–tin (Ni–Sn) alloy nanowires have been widely studied as potential superior anode material due to the high capacity of Ni–Sn alloy and the easy fabrication process [21,22]. Recently, we showed that the structural stability and electrochemical performance of Ni–Sn nanowire array electrode can be significantly improved by creating nanosized active/inactive interfaces at roots of nanowires to reduce the strain mismatch between active and inactive materials [23]. To further the development of high areal capacity Ni–Sn nanowire electrodes using longer Ni–Sn nanowires, a big challenge, agglomeration, is unavoidable. In this work, we focus on two objectives: (1) understanding the effect of nanowire agglomeration on Li-ion battery performance by systematically investigating the electrochemical performance of straight Ni–Sn nanowire arrays with different lengths and (2) constructing three-dimensional (3D) self-supporting Ni–Sn nanowire network electrodes to mitigate agglomeration based on our recently-developed 3D PAA template technique [24]. We found that although the electrochemical performance of straight nanowire array electrodes degrades as the nanowire length increases, the electrochemical performance of the

* Corresponding author. Tel.: +1 303 735 1003; fax: +1 303 492 3498.
E-mail addresses: mmtian@colorado.edu (M. Tian), ronggui.yang@colorado.edu (R. Yang).

0378-7753/$ – see front matter © 2012 Elsevier B.V. All rights reserved.
doi:10.1016/j.jpowsour.2012.03.084

3D Ni–Sn nanowire network electrodes are length-independent, which is attributed to their capability to mitigate agglomeration.

2. Experimental

2.1. Sample preparation

The PAA templates were prepared by anodizing Al sheets in phosphoric acid. The conventional PAA templates with straight nanochannels were synthesized by anodizing high-purity (99.999%) Al sheets at 180 V in 0.3 M phosphoric acid for 72 h at −3 °C, followed by channel widening in 3 wt.% phosphoric acid at 45 °C for 3 h 15 min [25]. The resulting PAA template has channels with diameters of ∼250 nm and an interchannel distance of ∼480 nm. The 3D PAA templates with nano-indentations along the nanochannels were synthesized by anodizing commercial low-purity 1000 series (99% purity, McMaster 9060K16) Al sheets at 170 V in 0.3 M phosphoric acid for 72 h at 5 °C, followed by channel widening in 3 wt.% phosphoric acid at 45 °C for 2 h [24]. The resulting 3D PAA template has channels with diameters of ∼240 nm and an interchannel distance of ∼460 nm. The characteristic size of the indentations in the nanochannels is ∼80 nm.

A two-step electrochemical deposition process was used to grow both straight Ni–Sn nanowire arrays and 3D Ni–Sn nanowire networks on Cu current collectors, which controls nanosized inactive/active interfaces by the growth of short Cu nanowires on the current collector before Ni–Sn electroplating (see Fig. S5 for illustration of the setup) [23]. The first step is to electrodeposit short Cu nanorods to bond the PAA template onto the Cu substrate (current collector). A sandwich structure that stacks the substrate (Cu current collector), PAA template, filter paper saturated with electrolyte, and counter-electrode in sequence was used in this step. A constant voltage of 0.8 V was applied between the Cu substrate and the counter-electrode for 10 min to grow short nanorods, which serve as "nanoscrews" to bond the PAA template onto the Cu substrate. The electrolyte consists of 6 g L^{-1} cupric pyrophosphate ($Cu_2P_2O_7 \cdot xH_2O$; Sigma–Aldrich 344699), 25 g L^{-1} potassium pyrophosphate ($K_4P_2O_7$, Sigma–Aldrich 322431), and 2 g L^{-1} ammonium citrate ($C_6H_{17}N_3O_7$, Fluka 09831) [26]. In the second electrodeposition step, Ni–Sn nanowires were synthesized by co-depositing Sn and Ni in a three-electrode glass cell at −1 V (vs. Ag/AgCl reference electrode) with the Cu substrate bonded with the PAA template as working electrode and a Pt coil as the counter-electrode. The electrolyte consists of 17.82 g L^{-1} $NiCl_2 \cdot 6H_2O$, 39.4 g L^{-1} $SnCl_2 \cdot 2H_2O$, 165.15 g L^{-1} $K_4P_2O_7$, and 9.38 g L^{-1} glycine, with an addition of NH_4OH 5 mL L^{-1} for pH value control [21,27]. The potentiostatic deposition was performed on a CHI 760c electrochemical work station. Finally, the Ni–Sn nanowire samples were immersed in 1 M NaOH solution to dissolve the PAA templates and cleaned with deionized water. The composition of both Ni–Sn nanowire

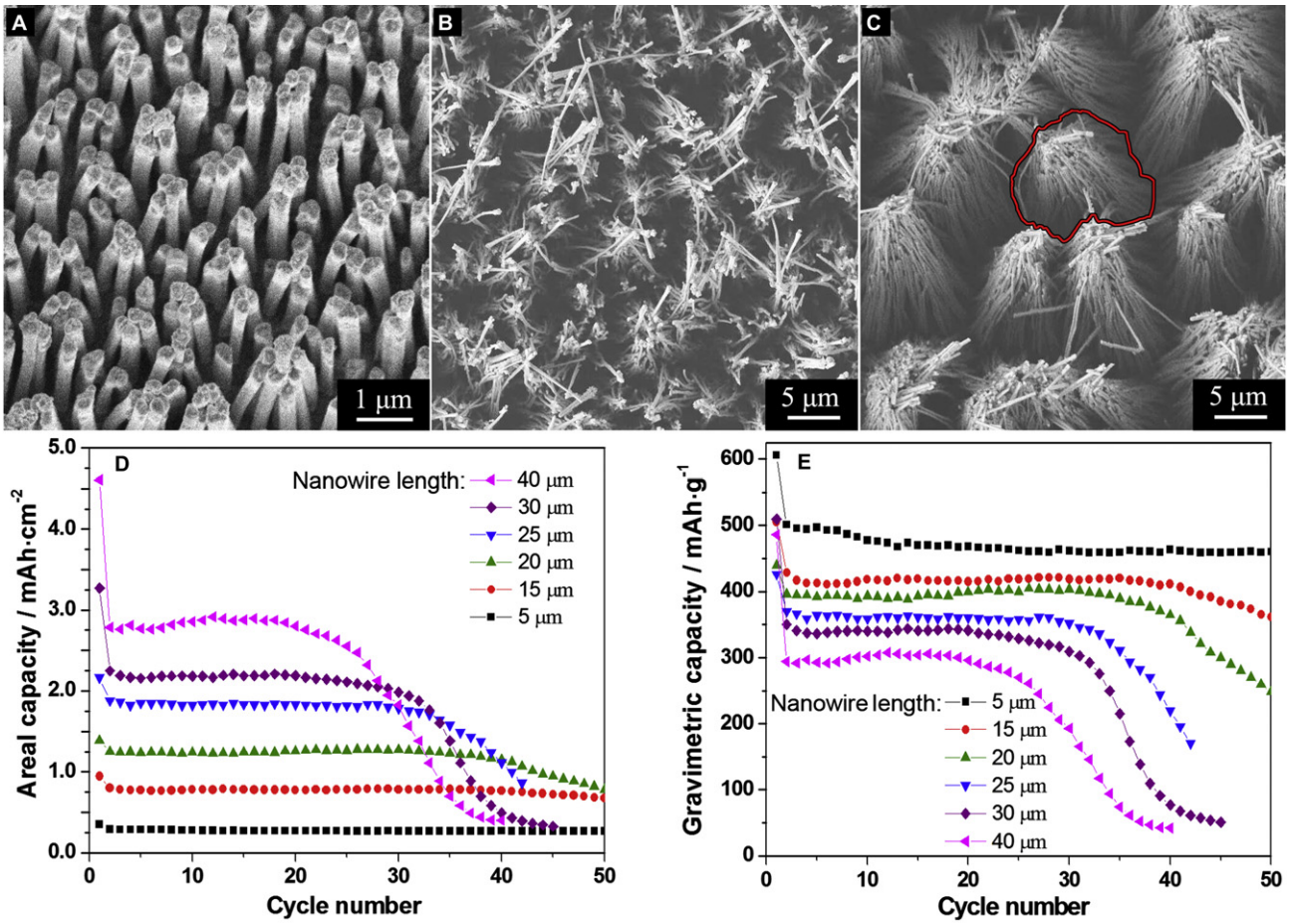

Fig. 1. Top-view FE-SEM micrographs of straight Ni–Sn nanowire arrays with lengths of A) 5 μm, B) 20 μm, and C) 40 μm. One agglomerated nanowire bundle is circled in red in C). D) Areal capacity and E) gravimetric capacity of Ni–Sn straight nanowires with different lengths. The test rate is set at C/5. (For interpretation of the references to color in this figure legend, the reader is referred to the web version of this article.)

arrays and 3D Ni–Sn nanowire networks are similar, with around 87 wt.% Sn, using this two-step electrochemical deposition process.

2.2. Structure characterizations

The field emission scanning electron microscope (FE-SEM, JEOL JSM-7401F) was employed to study the morphology of the Ni–Sn nanowires. Cross-sectional images of nanowires were taken by tearing the samples apart and mounting them on a tilted SEM stage. An X-ray diffraction spectrometer (Scintag PAD5) with Cu Kα radiation (1.54056 Å) was used to record the XRD patterns.

2.3. Electrochemical characterizations

The as-prepared Ni–Sn nanowire samples were tested in an electrolyte containing 1 M $LiPF_6$ in ethylene carbonate (EC)/dimethyl carbonate (DMC) (1:1 volume ratio, Aldrich), with Li foil (Alfa Aesar) as counter-electrode. The CR2032 coin-type cells were assembled in an argon-filled glove box system (Vacuum Atmosphere Nexus model) and tested with a computer controlled potentiostats/galvanostats system (MTI, 5V1mA). The discharge–charge experiments were performed galvanostatically within the voltage window of 0.01–1.5 V (vs. Li/Li+). The gravimetric capacity is calculated with respect to the mass of the Ni–Sn alloy.

3. Results and discussion

3.1. Performance degradation of straight Ni–Sn nanowire arrays

To study the effects of agglomeration on the electrochemical performance of straight Ni–Sn nanowire array electrodes, straight Ni–Sn nanowire arrays were fabricated by electrodeposition of intermetallic Ni–Sn into conventional porous anodic alumina (PAA) templates with straight nanochannels [28–31], followed by dissolving the PAA templates in a NaOH solution (see Experimental section for details). The high surface tension of water causes agglomeration of nanowires when the nanowires are released and dried. Fig. 1A–C shows top-view field emission scanning electron microscope (FE-SEM) micrographs of Ni–Sn nanowire arrays with lengths of 5 μm, 20 μm, and 40 μm. Clearly the nanowires agglomerated into micron-size bundles. More severe agglomeration is observed in longer nanowire arrays due to their higher aspect ratio and lower stiffness. The average diameters of the agglomerated nanowire bundles increase from 1.5 μm to 19 μm when the nanowire length increases from 5 μm to 40 μm. Apparently, more nanowires are in contact with one another in larger

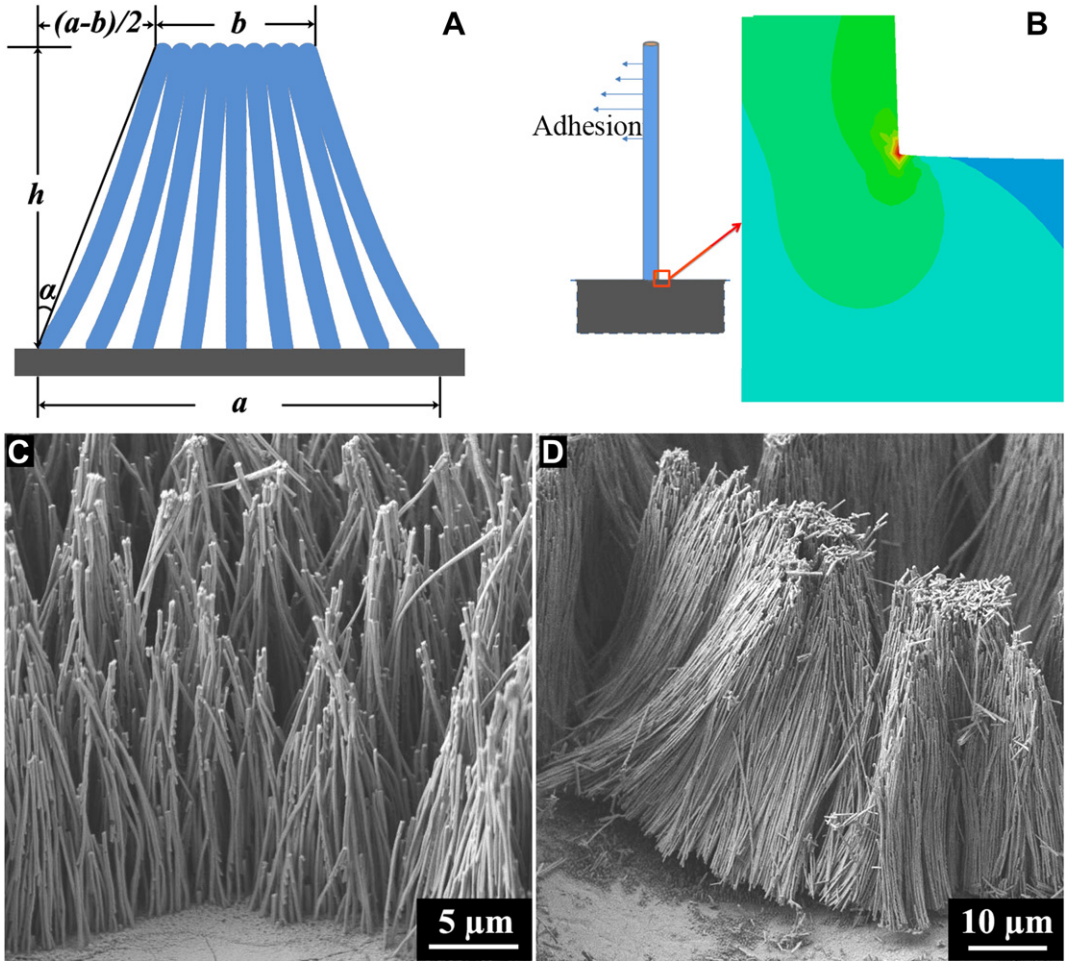

Fig. 2. A) Schematic of an agglomerated nanowire bundle. B) The clamped beam model used to study the stress in a bent nanowire and the principal stress contours at the root of a nanowire. The colors from red to blue correspond to stress concentrations from highest to lowest. Cross-sectional FE-SEM micrographs of Ni–Sn nanowire bundles with nanowire lengths of C) 20 μm and D) 40 μm. (For interpretation of the references to color in this figure legend, the reader is referred to the web version of this article.)

Table 1
Agglomeration-induced inclination of nanowire arrays.

h/μm	a/μm	b/μm	α/°
5	1.5	0.85	3.7
20	6	2.3	5.3
25	9.5	4	6.3
40	19	5	10

agglomerated nanowire bundles, which results in larger surface area loss in longer nanowire arrays.

In Fig. 1D, areal discharging capacities of Ni–Sn nanowire arrays with different nanowire lengths are compared. In general, the areal capacity of Ni–Sn nanowire array electrodes increases when the nanowire length increases, due to the mass-loading increase of the active material. The 40-μm-long Ni–Sn nanowire electrode can deliver a reversible areal capacity as high as 2.8 mAh cm^{-2}, which is 6.2 times that of the Ni–Sn film reported by Hassoun et al. [32] (0.45 mAh cm^{-2}) and 10.4 times that of the 5-μm-long Ni–Sn nanowires (0.27 mAh cm^{-2}). This observation confirms that longer Ni–Sn nanowires can increase the areal capacity of nanowire array electrodes.

However, because of the agglomeration of straight nanowire arrays, the gravimetric capacity and the cycle life of the electrodes degrade significantly when the nanowire length increases, as shown in Fig. 1E. The gravimetric capacity of the Ni–Sn nanowire electrodes decreases from ~470 mAh g^{-1} to ~300 mAh g^{-1} when the nanowire length increases from 5 μm to 40 μm. The stability of the electrodes also decreases when the nanowire length increases. The 5-μm-long nanowire electrode lasted over 50 cycles with 92% of the second-cycle capacity retained, while the 40-μm-long nanowire electrode lasted only around 25 cycles before the capacity dropped dramatically. The loss of gravimetric capacity is due to (1) the limited access of the electrolyte to the active material caused by the loss of surface area, and (2) the long Li-ion diffusion path caused by the increase of the nanowire bundle size.

To understand the mechanisms underlying the degraded cycle life in the agglomerated Ni–Sn nanowires, we have carefully examined the agglomerated nanowire bundles. We use Fig. 2A to illustrate a micro-sized bundle of the agglomerated nanowires shown in Fig. 1A–C. The cross section of an agglomerated nanowire bundle can be simplified as an isosceles trapezoid, with the long base a (the average diameter of agglomerated nanowire bundle), the height h (the length of the nanowires), and the short base b (the diameter of the bundle top area). The inclination angle α of the nanowires at the edge of bundles can be approximated as $\alpha = \tan^{-1}[(a-b)/2h]$. As summarized in Table 1, α becomes larger when the nanowire length increases. If we think of a nanowire bent by adhesion as a clamped beam subjected to a moment M at its free end, M is proportional to the inclination α. Clearly, the data presented in Table 1 indicate that longer nanowires are subjected to larger bending due to agglomeration. In general, the most severe

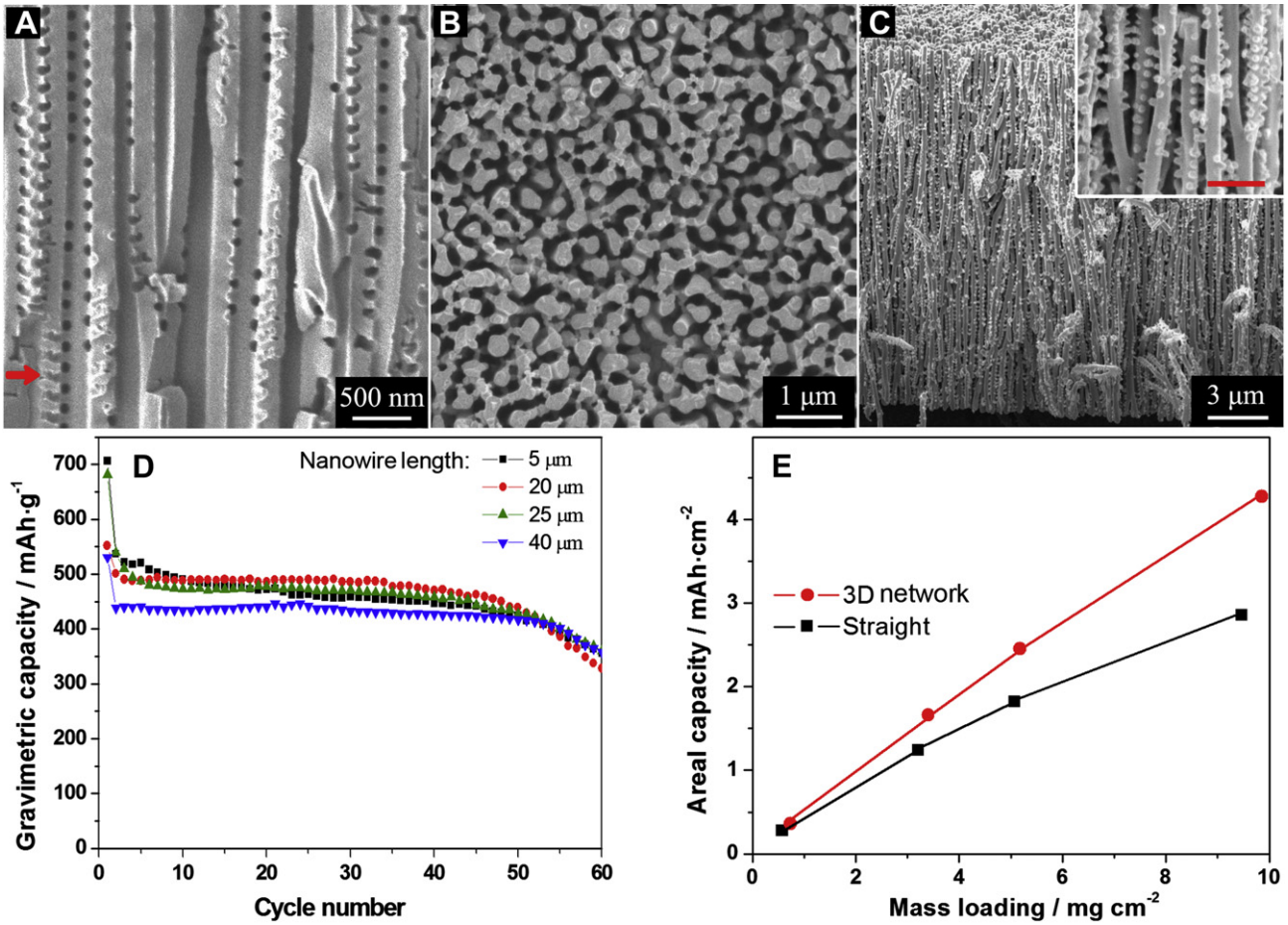

Fig. 3. A) Cross-sectional FE-SEM micrograph of a 3D PAA template. B) Top-view and **C**) cross-sectional FE-SEM micrographs of a 20-μm-long 3D Ni–Sn nanowire network. Inset: higher magnification image of nanowires with the scale bar indicating 1 μm. D) Gravimetric capacities of 3D Ni–Sn nanowire networks with different lengths. E) Areal capacity (at the 10th cycle) as a function of mass loading of active material in straight Ni–Sn nanowire arrays and 3D Ni–Sn nanowire networks. The test rate is set at C/5.

stress concentration occurs at the root of a bent nanowire, as demonstrated in the finite-element analysis shown in Fig. 2B (see Supporting information for simulation details). The principal stress contour shows that the stress concentrates at the root of the nanowire due to agglomeration-induced bending. Bear in mind that the stress concentration level is proportional to the applied moment in linear elastic problems; higher stresses are concentrated at the root of longer nanowires due to agglomeration. This mechanical analysis is confirmed by the micro-structural analysis. In Fig. 2C, the 20-μm-long Ni–Sn nanowires have good connections to the substrate before the cycling processes. In contrast, in the 40-μm-long Ni–Sn nanowire sample shown in Fig. 2D, we can clearly observe that some peeled off at the edge of the micro-sized bundles, which experience the most severe mechanical stress due to agglomeration. Earlier works on Ni–Sn nanowire array electrodes showed that reliable electrical connection between the nanowires and the current collector is one of the keys to obtaining a stable electrode [23,33]. The mechanical analysis here proves that the high stress-induced fatigue at the interface between the Ni–Sn nanowires and the Cu substrate is the cause of the shorter cycle life observed in the longer Ni–Sn nanowire arrays [34].

In short, agglomeration greatly degrades the capacity and the cycle life of straight Ni–Sn nanowire arrays when the nanowire length increases, by degrading the nanoscale wires to micro-sized bundles and reducing the mechanical stability.

3.2. Performance improvement of 3D Ni–Sn nanowire networks

To mitigate the serious agglomeration of straight Ni–Sn nanowire arrays and to improve the electrochemical performance of nanowire electrodes, in this study we propose to use 3D Ni–Sn nanowire networks as Li-ion battery electrodes. We use a process similar to the synthesis of straight nanowire arrays for the preparation of 3D Ni–Sn nanowire networks, but with unconventional PAA templates synthesized using low-cost impure Al sheets. Nano-indentations in nanochannels of PAA templates have been reported when anodizing low-purity Al sheets and are regarded as defects [35,36]. In this study, we utilize the defect-containing PAA templates to fabricate 3D Ni–Sn nanowire networks. To distinguish them from the conventional PAA templates used to fabricate straight nanowires, we call these defect-containing PAA templates synthesized from low-purity Al sheets 3D PAA templates. Fig. 3A shows the cross-sectional FE-SEM micrograph of a 3D PAA template we prepared by anodizing a 99% Al sheet. Beside the parallel nanochannels with diameters of ~240 nm, there are abundant nano-indentations with a characteristic size of ~80 nm on the walls of the straight nanochannels. Some of the nanochannels are even connected by the indentations, as indicated by an arrow in Fig. 3A. Such 3D PAA templates have been used to fabricate 3D Ni–Sn nanowire networks. Fig. 3B and C shows top-view and cross-sectional images of a 3D Ni–Sn nanowire network fabricated by electrodepositing Ni–Sn alloy in a 3D PAA template and subsequently removing the template. In contrast to the straight Ni–Sn nanowire arrays shown in Fig. 1A–C, the 3D Ni–Sn nanowires are uniformly spaced as shown in Fig. 3B, which clearly demonstrates the elimination of agglomeration. We note that 3D Ni–Sn nanowire networks with different nanowire lengths from 5 μm to 40 μm have similar top-view images. In Fig. 3C, the straight vertical nanowires are clearly connected with each other by the horizontal "bridges" which result from the nano-indentations in the 3D PAA templates. These bridges not only stiffen the nanowire network structures and prevent agglomeration, but also provide connections between nanowires to facilitate the electron transport in the electrodes of Li-ion batteries [33,37–40]. In addition, the elimination of agglomeration in 3D Ni–Sn nanowire networks releases the stress at the roots of the nanowires, stabilizing the connection of the nanowires to the current collector.

Table 2
Mass loading of active material in Ni–Sn nanowire electrodes.

Straight nanowire arrays		3D nanowire networks	
Lengh/μm	Mass loading/mg cm^{-2}	Length/μm	Mass loading/mg cm^{-2}
5	0.58	5	0.73
20	3.21	20	3.4
25	5.08	25	5.18
40	9.47	40	9.86

All the 3D Ni–Sn nanowire networks with different nanowire lengths from 5 μm to 40 μm deliver similar gravimetric capacity with similar cycle life as shown in Fig. 3D, in contrast to the dramatic decrease of cycle life and gravimetric capacity when increasing the nanowire length in straight Ni–Sn nanowire arrays (see Fig. S4 for comparison of charge/discharge curves). Apparently, by eliminating agglomeration, the stress concentration at the roots of the nanowires due to bending has been effectively released, which improves the stability of the nanowires. High gravimetric capacity of ~450 mAh g^{-1} is retained in 3D Ni–Sn nanowire networks even when the nanowire length is increased to 40 μm. This improvement mainly comes from the preservation of the large specific surface area and the short Li-ion diffusion path in long nanowire networks [41]. The retention of high gravimetric capacity in long 3D Ni–Sn nanowire networks enables the realization of high areal capacity by increasing the mass loading of the active material. Fig. 3E shows that the areal capacity of the 3D Ni–Sn nanowire networks increases almost linearly with the mass loading of active material (see Table 2 for the mass loadings of nanowires with different lengths). In contrast, the rate of the areal capacity increase drops when the mass loading is increased in the straight Ni–Sn nanowire array electrodes. For example, the areal capacity of the 40-μm-long 3D Ni–Sn nanowire network is 4.3 mAh cm^{-2}, which is 1.5 times that of the 40-μm-long straight Ni–Sn nanowire arrays (2.8 mAh cm^{-2}), although the mass loadings are similar in these two long nanowire samples.

Besides the enhanced capacity and much longer cycle life, the 3D Ni–Sn nanowire networks also show much better rate capability than the straight nanowire arrays, as shown in Fig. 4. When increasing the test rate from C/10 to 6C, the 20-μm-long straight Ni–Sn nanowire array electrode can only retain 15% of its initial

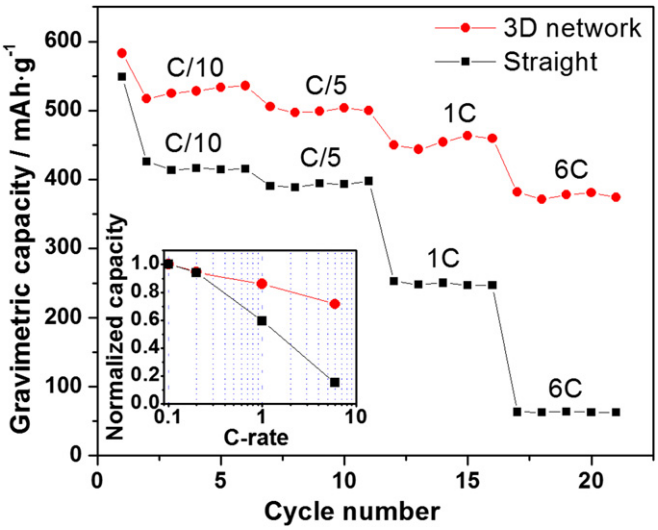

Fig. 4. Areal discharging capacities of the 20-μm-long straight Ni–Sn nanowire array and 3D Ni–Sn nanowire network at different test rates. Inset: normalized capacity vs. test rate.

capacity. In contrast, the 20-μm-long 3D Ni–Sn nanowire network electrode can keep 72% of its initial capacity. The excellent rate capability of 3D Ni–Sn nanowire networks is a result of fast Li-ion transfer to the electrode due to the stable nanoscale space between nanowires, fast electrode reactions due to the large surface area, and the short Li-ion diffusion paths due to the small diameters [42].

4. Conclusions

In summary, we have systematically studied the effect of agglomeration on the electrochemical performance of straight Ni–Sn nanowire array anodes. Due to agglomeration, the gravimetric capacity becomes lower and the cycle life becomes shorter when the nanowire length increases from 5 μm to 40 μm in straight nanowire array anodes. To mitigate the agglomeration of nanowire arrays, we have successfully fabricated 3D Ni–Sn nanowire networks. With preservation of the uniform spacing between nanowires and the nanoscale Li-ion diffusion paths, we have realized linear increase of areal capacity with respect to mass loading of active material in 3D Ni–Sn nanowire network electrodes. The cycle life of the 3D nanowire network electrodes has been prolonged due to the release of the stress at the roots of the self-supporting nanowire networks. An areal capacity as high as 4.3 mAh cm^{-2} has been demonstrated in the 3D Ni–Sn nanowire network electrode with a nanowire length of 40 μm, which is 1.5 times that of the straight nanowire array electrode with the same length. The cycle life has been doubled to be longer than 50 cycles. In addition, the 3D Ni–Sn nanowire network exhibits an excellent rate capability with 72% of the capacity retained when the test rate increases from C/5 to 6C. This research paves the way for developing on-chip high energy and high power microbatteries.

Acknowledgment

This work was supported by a University of Colorado Innovative Seed Grant and the Defense Advanced Research Projects Agency (DARPA) N/MEMS S&T Fundamentals program through the DARPA Center on Nanoscale Science and Technology for Integrated Micro/Nano-Electromechanical Transducers (iMINT) under grant No. N66001-10-1-4007 issued by the Space and Naval Warfare Systems Center Pacific (SPAWAR). Part of the fabrication was conducted at the Colorado Nanofabrication Laboratory, supported by the NNIN and the National Science Foundation under Grant No. ECS-0335765.Y. W. also acknowledges the support from Chinese Academy of Sciences via the “Hundred Talent program” and support from NSFC (No. 11021262).

Appendix A. Supplementary data

Supplementary data associated with this article can be found, in the online version, at doi:10.1016/j.jpowsour.2012.03.084.

References

[1] J.M. Tarascon, M. Armand, Nature 414 (2001) 359–367.
[2] A.S. Arico, P. Bruce, B. Scrosati, J.M. Tarascon, W. Van Schalkwijk, Nat. Mater. 4 (2005) 366–377.
[3] Y.G. Guo, J.S. Hu, L.J. Wan, Adv. Mater. (Weinheim, Ger.) 20 (2008) 2878–2887.
[4] F. Cheng, Z. Tao, J. Liang, J. Chen, Chem. Mater. 20 (2008) 667–681.
[5] A.R. Armstrong, G. Armstrong, J. Canales, P.G. Bruce, J. Power Sources 146 (2005) 501–506.
[6] Y.G. Li, B. Tan, Y.Y. Wu, J. Am. Chem. Soc. 128 (2006) 14258–14259.
[7] A.R. Armstrong, G. Armstrong, J. Canales, R. Garcia, P.G. Bruce, Adv. Mater. (Weinheim, Ger.) 17 (2005) 862–865.
[8] C.K. Chan, R.N. Patel, M.J. O'Connell, B.A. Korgel, Y. Cui, ACS Nano 4 (2010) 1443–1450.
[9] Y. Cui, Nat. Nanotechnol. 3 (2008) 31.
[10] G. Ferrara, L. Damen, C. Arbizzani, R. Inguanta, S. Piazza, C. Sunseri, M. Mastragostino, J. Power Sources 196 (2011) 1469–1473.
[11] H. Ghassemi, M. Au, N. Chen, P.A. Heiden, R.S. Yassar, ACS Nano 5 (2011) 7805–7811.
[12] Y.G. Li, B. Tan, Y.Y. Wu, Nano Lett. 8 (2008) 265–270.
[13] R. Teki, M.K. Datta, R. Krishnan, T.C. Parker, T.-M. Lu, P.N. Kumta, N. Koratkar, Small 5 (2009) 2236–2242.
[14] L.-F. Cui, R. Ruffo, C.K. Chan, H. Peng, Y. Cui, Nano Lett. 9 (2008) 491–495.
[15] P.L. Taberna, S. Mitra, P. Poizot, P. Simon, J.M. Tarascon, Nat. Mater. 5 (2006) 567–573.
[16] X.D. Wu, H. Li, L.Q. Chen, X.J. Huang, Solid State Ionics 149 (2002) 185–192.
[17] J. Kim, S. Khanal, M. Islam, A. Khatri, D. Choi, Electrochem. Commun. 10 (2008) 1688–1690.
[18] P.G. Bruce, B. Scrosati, J.-M. Tarascon, Angew. Chem. Int. Ed. 47 (2008) 2930–2946.
[19] T. Takamura, M. Uehara, J. Suzuki, K. Sekine, K. Tamura, J. Power Sources 158 (2006) 1401–1404.
[20] S.W. Lee, N. Yabuuchi, B.M. Gallant, S. Chen, B.S. Kim, P.T. Hammond, Y. Shao-Horn, Nat. Nanotechnol. 5 (2010) 531–537.
[21] J. Hassoun, S. Panero, P. Simon, P.L. Taberna, B. Scrosati, Adv. Mater. (Weinheim, Ger.) 19 (2007) 1632–1635.
[22] M. Kotobuki, N. Okada, K. Kanamura, Chem. Commun. (Cambridge, U. K.) 47 (2011) 6144–6146.
[23] M. Tian, W. Wang, S.H. Lee, Y.C. Lee, R.G. Yang, J. Power Sources 196 (2011) 10207–10212.
[24] W. Wang, M. Tian, A. Abdulagatov, S.M. George, Y.-C. Lee, R. Yang, Nano Lett. 12 (2011) 655–660.
[25] M.S. Sander, A.L. Prieto, R. Gronsky, T. Sands, A.M. Stacy, Adv. Mater. (Weinheim, Ger.) 14 (2002) 665–667.
[26] A. Bund, D. Thiemig, J. Appl. Electrochem. 37 (2007) 345–351.
[27] H. Mukaibo, T. Momma, M. Mohamedi, T. Osaka, J. Electrochem. Soc. 152 (2005) A560–A565.
[28] S. Zhao, K. Chan, A. Yelon, T. Veres, Nanotechnology 18 (2007) 245304.
[29] H. Masuda, K. Fukuda, Science 268 (1995) 1466–1468.
[30] B. Luo, D.C. Yang, M.H. Liang, L.J. Zhi, Nanoscale 2 (2010) 1661–1664.
[31] A.L.M. Reddy, M.M. Shaijumon, S.R. Gowda, P.M. Ajayan, Nano Lett. 9 (2009) 1002–1006.
[32] J. Hassoun, S. Panero, B. Scrosati, J. Power Sources 160 (2006) 1336–1341.
[33] J. Xie, X. Yang, S. Zhou, D. Wang, ACS Nano 5 (2011) 9225–9231.
[34] J.P. Rong, C. Masarapu, J. Ni, Z.J. Zhang, B.Q. Wei, ACS Nano 4 (2010) 4683–4690.
[35] I.S. Molchan, T.V. Molchan, N.V. Gaponenko, P. Skeldon, G.E. Thompson, Electrochem. Commun. 12 (2010) 693–696.
[36] D. Lo, R.A. Budiman, J. Electrochem. Soc. 154 (2007) C60.
[37] K.G. Biswas, H. El Matbouly, V. Rawat, J.L. Schroeder, T.D. Sands, Appl. Phys. Lett. 95 (2009) 073108.
[38] H. Zhang, X. Yu, P. Braun, Nat. Nanotechnol. 6 (2011) 277–281.
[39] M. Rauber, I. Alber, S. Muller, R. Neumann, O. Picht, C. Roth, A. Schokel, M.E. Toimil-Molares, W. Ensinger, Nano Lett. 11 (2011) 2304–2310.
[40] Y. Yao, K. Huo, L. Hu, N. Liu, J.J. Cha, M.T. McDowell, P.K. Chu, Y. Cui, ACS Nano 5 (2011) 8346–8351.
[41] P. Kubiak, T. Froschl, N. Husing, U. Hormann, U. Kaiser, R. Schiller, C.K. Weiss, K. Landfester, M. Wohlfahrt-Mehrens, Small 7 (2011) 1690–1696.
[42] J.S. Sakamoto, B. Dunn, J. Mater. Chem. 12 (2002) 2859–2861.